EFDA–JET–PR(13)63

L. Frassinetti, D. Dodt, M.N.A. Beurskens, A Sirinelli, J.E. Boom, T. Eich,
J. Flanagan, C. Giroud, M.S. Jachmich, M. Kempenaars, P. Lomas,
G. Maddison, C. Maggi, R. Neu, I. Nunes, B. Sieglin, M.Stamp
and JET EFDA contributors

Effect of Nitrogen Seeding on the ELM Energy Losses in JET with the ITER-Like Wall

Effect of Nitrogen Seeding on the ELM Energy Losses in JET with the ITER-Like Wall

L. Frassinetti[1], D. Dodt[2], M.N.A. Beurskens[3], A Sirinelli[3], J.E. Boom[2], T. Eich[2], J. Flanagan[3], C. Giroud[3], M.S. Jachmich[3], M. Kempenaars[3], P. Lomas[3], G. Maddison[3], C. Maggi[2], R. Neu[2,4], I. Nunes[5], B. Sieglin[2], M.Stamp[3] and JET EFDA contributors*

JET-EFDA, Culham Science Centre, OX14 3DB, Abingdon, UK

[1]Division of Fusion Plasma Physics, Association EURATOM-VR , KTH, SE-10044 Stockholm, Sweden
[2]Max-Planck-Institut für Plasma Physik, Boltzmannstr.2, 85748 Garching, Germany
[3]EURATOM /CCFE Fusion Association, Culham Science Centre, Abingdon, OX14 3DB, UK
[4]Technische Universität München, Boltzmannstr. 15, 85748 Garching, Germany
[5]Centro de Fusao Nuclear, Associacao EURATOM-IST, Lisboa, Portugal
** See annex of F. Romanelli et al, "Overview of JET Results",*
(24th IAEA Fusion Energy Conference, San Diego, USA (2012)).

Preprint of Paper to be submitted for publication in
Nuclear Fusion

ABSTRACT

The baseline type I ELMy H-mode scenario has been re-established in JET with the new tungsten MKII-HD divertor and beryllium on the main wall (hereafter called ITER-like wall, JET-ILW).

The first JET-ILW results show that the confinement is degraded by 20–30% in the baseline scenarios compared to the previous carbon wall JET (JET-C) plasmas [13]. The degradation is mainly driven by the reduction in the pedestal temperature. Stored energies and pedestal temperature comparable to the JET-C have been obtained in JET-ILW baseline plasmas only in the high triangularity shape using N_2 seeding [13].

This work compares the pedestal behaviour and the energy losses during ELMs in JET-ILW baseline plasmas with and without N_2 seeding with similar JET-C baseline plasmas. ELMs in the JET-ILW differ from those with the carbon wall both in terms of time scales and energy losses. The ELM time scale, defined as the time to reach the minimum pedestal temperature soon after the ELM collapse, are ≈ 2ms in the JET-ILW and lower than 1ms in the JET-C. The energy losses relative to the pedestal energy are $\Delta W_{ELM}/W_{ped} \approx 7–12\%$ in the JET-ILW and $\Delta W_{ELM}/W_{ped} \approx 10–20\%$ in JET-C. In both cases, the energy losses fit relatively well with earlier multi-machine empirical scalings of $\Delta W_{ELM}/W_{ped}$ with collisionality [17]. The time scale of the ELM collapse seems to be related to the pedestal collisionality. However, most of the non-seeded JET-ILW ELMs are followed by a further energy drop characterized by a slower time scale ≈ 10–15ms (hereafter called slow transport events), that can lead to losses in the range $\Delta W_{slow}/W_{ped} \approx 15–22\%$, i.e. slightly larger than the JET-C ELM energy losses. On the other hand, the JET-ILW plasmas with N_2 seeding have a ELM behaviour similar to the JET-C, both in terms of time scales, energy losses and absence of the slow transport events.

INTRODUCTION

Tokamak plasmas in the H-mode regime are characterized by periodic edge localized modes (ELMs) that produce the partial collapse of the pedestal pressure and the consequent release of energy and particles towards the wall and the divertor targets. Material studies [29] have shown that in ITER the maximum tolerable ELM energy loss (ΔW_{ELM}) is approximately 1MJ for the baseline $Q_{DT} = 10$ ITER scenario, corresponding to approximately 1% of the ITER pedestal stored energy (W_{ped}). A multi-device study performed on DIII-D, ASDEX, JT60U and on the carbon wall JET (hereafter JET-C) has shown that the relative ELM energy losses scale with the inverse of the pedestal collisionality [17] predicting large losses for the ITER target collisionality with $\Delta W_{ELM}/W_{ped} > 15\%$.

To reduce the long term tritium retention, ITER will not operate with a carbon wall but with beryllium in the main chamber and tungsten in the divertor. In order to study the effects of the plasma on these materials and to improve the prediction for ITER, the carbon wall in JET-C has been replaced in 2010 by an ITER-like wall (JET-ILW) with mostly Be in the main chamber and W in the divertor [8, 19]. ASDEX Upgrade operates with a DEMO-relevant full W wall since approximately 2007 [20].

The initial results obtained in the JET-ILW have shown that the first wall material seems to affect

both the plasma confinement and the pedestal properties especially in the ITER baseline scenarios [13, 6]. The plasma confinement factor H_{98} (defined as the ratio between the energy confinement and the confinement expected from a multi-machine scaling [14]) to achieve the ITER baseline scenarios is $H_{98} = 1$ in the type-I ELMy H-mode plasma. The JET-C has achieved $H_{98} = 1$ both in a low and a high triangularity plasma shape [21, 23, 5], but with the high shape characterized by a better confinement at a given Greenwald density due to the improved pedestal stability. To date, the JET-ILW standard baseline plasma has not routinely achieved a confinement factor $H_{98} = 1$, but is characterized by a confinement factor in the range $H_{98} = 0.8–0.9$ for both low and high triangularity with no significant confinement improvement for the high shape plasmas. The degraded confinement is mainly driven by a lower pedestal pressure due to a pedestal temperature approximately 20–30% lower than in JET-C. The pedestal density is instead comparable among JET-C and JET-ILW. To date, a JET-ILW pedestal pressure comparable to the baseline JET-C has been achieved only in high triangularity experiments with N_2 seeding [11, 13]. Interestingly, JET-C plasmas with N_2 seeding have shown no confinement improvement compared to the non-seeded JET-C plasmas [12].

The metal wall has produced confinement degradation also in ASDEX Upgrade with a partial recovery of the confinement obtained with N_2 seeding [26]. As discussed in detail in [7], the confinement degradation with a metal wall and its partial recovery with N_2 cannot be ascribed to a core effect, as the core temperature gradient lengths are comparable and can be only partially ascribed to a pedestal ion-dilution effect due to the change of the impurities in the plasma. The mechanism that regulates the pedestal confinement degradation with a metal wall and its partial recovery with N_2 seeding is still under investigation. Studies on the ELM dynamics in ASDEX Upgrade with and without N_2 seeding are described in [25].

The aim of this work is to characterize the ELM energy losses in the non-seeded and nitrogen seeded JET-ILW plasmas and to compare the results with similar JET-C plasmas in order to investigate if the current predictions for ELM energy loss in ITER will be affected by the metal wall.

The H-mode plasmas studied in this work are mainly in the Type-I ELM regime. Type-I ELMy H-modes are characterized by the increase of the ELM frequency (f_{ELM}) with the input power [24] and by relatively large energy losses ($\Delta W_{ELM}/W_{tot} > 1\%$), while Type-III ELMy H-modes are characterized by the f_{ELM} reduction with the input power and by relatively small energy losses. JET-C plasmas can also be characterized by mixed Type I/II ELMs [23, 15]. A pure Type II regime is classified by the absence of large transient heat loads and by the absence of type I ELMs, producing a continuous heat load on the divertor region. Pure type II ELMs have been observed in ASDEX-Upgrade [28], but in JET only a mixed type I/II regime has been observed. The transition to a mixed type I/II ELMy H-mode can occur at high pedestal densityes ($n_e \geq 0.7–0.8 n_{GW}$), and is accompanied by a reduction of the ELM frequency compared to the pure type I ELMs.

The JET-C plasmas here analysed are mainly characterized by Type I ELMs excluding one set of shots which is likely in the mixed Type I-II regime. The reason for including this set is discussed in Section 2. The JET-ILW plasmas are characterized Type I ELMs. The results presented in the gas scan

described in [4, 6] suggest that the threshold between Type I and Type III ELMs is approximately $T_e^{ped} \approx 300$eV in the JET-ILW, well below the pedestal temperature of the shots analysed in this work. Moreover, as later described, the JET-ILW ELM energy losses are relatively large when compared to the typical Type-III energy losses, confirming that the present JET-ILW data set is composed of Type-I ELMs.

The temperature data analysed in this work are measured by the electron cyclotron emission (ECE) radiometer [9] with a time resolution up to 4ms. The radial position of the ECE data has been calculated at each time step using the magnetic field from the fast EFIT equilibrium and then mapped on ρ_θ (the square root of the poloidal flux). As described in detail in reference [1], a correction factor in the vacuum magnetic field is necessary to match the ECE temperature profiles with those measured from the High Resolution Thomson Scattering (HRTS). For the plasmas analysed in this work, the correction factor is less than 1%. The density data are measured by the reflectometer with a time resolution up to 15ms [27]. The radial position of the reflectometer data have been mapped at each time step on ρ_θ using the fast EFIT equilibrium. When ECE radiometer and/or reflectomer were not available, the High Resolution Thomson Scattering (HRTS) [22, 10] has been used.

The paper is organized as follows. In Section 2, the data set used in this work is described along with the characterization of the electron pedestal temperature (T_e^{ped}) and density (n_e^{ped}) for all the shots. The pedestal time evolution during ELMs for three representative shots and the ELM time scales, defined as the time to reach the minimum after the pedestal collapse, are described and compared between JET-C and JET-ILW in Section 3. Section 4 describes the T_e and n_e profiles before and after the ELMs and compares the temperature and density pedestal collapses in JET-C and JET-ILW. Section 5 compares the ELM energy losses considering both the conductive and convective channels. The ELMs in the non-seeded JET-ILW are often followed by a further energy collapse characterized by a time scale slower than the standard ELM. These events will be discussed in Section 6. Finally, Section 7 discusses the results in light of the previous multi-machine collisionality scaling [17] and Section 8 presents the conclusions.

2. PEDESTAL HEIGHT IN JET-C AND JET-ILW

In JET, the metal wall has a detrimental effect on the confinement of baseline plasmas, with a H_{98} reduction from ≈ 1.0 in JET-C to ≈ 0.8–0.9 in JET-ILW. The confinement degradation is mainly driven by a $\approx 20\%$ reduction of the pedestal temperature [13, 6]. Pedestal pressures comparable to JET-C have been achieved in JET-ILW only in high triangularity N_2 seeded plasmas [13].

The experimental sessions with N_2 seeding in JET-ILW have been performed with plasma current 2.5MA, magnetic field 2.7T and NBI power 15–17MW. The non-seeded plasma analysed in this work have been selected in order to have the same current, field and power, both for JET-ILW and JET-C. A match in the main gas flow (deuterium, Γ_{D2}) between JET-ILW and JET-C is more complicated to obtain. With the metal wall, high temperatures in the SOL lead to increased tungsten sputtering which in turn can lead to an increased W-influx and eventually to W accumulation in the

plasma core producing hollow T_e profiles and leading to disruptions. To minimize the W-influx, JET-ILW tends to operate with a deuterium gas dosing larger than in the typical JET-C plasmas. The gas flow of the shots analysed in this work is in the range $\Gamma_{D2} = 2–2.5\ 10^{22}$ (e/s) for the high triangularity plasmas and $\Gamma_{D2} = 0.8–1.6\ 10^{22}$ (e/s) for the low triangularity plasmas for both JET-C and JET-ILW. However, for the high triangularity case, these Γ_{D2} levels are indeed larger than those typically used in JET-C, therefore a further set of high-δ JET-C shots with the typical fuelling level ($\Gamma_{D2} \approx 0.3\ 10^{22}$ e/s) is considered. The JET-C shots with low Γ_{D2} are characterized by type I ELMs while those with high Γ_{D2} show a lower ELM frequency and a pedestal density close to the Greenwald limit therefore suggesting a mixed type I/II regime. The JET-ILW plasmas are characterized by Type I ELMs [13]. The nitrogen rate in the seeded JET-ILW plasmas is different fro shot to shot and is in the range $\Gamma_{N2} = 0.5–3 \cdot 10^{22}$ (e/s). Some of the main plasma parameters for the seven groups analysed are summarized in Table 1.

The corresponding pedestal heights for electron temperature and density, T_e^{ped} and n_e^{ped} respectively, are shown in figure 1. The pedestal heights are calculated using the HRTS by selecting for each shot the profiles in the pre-ELM phase (within the 70% to 99% time interval of the ELM cycle).

The JET-C plasmas have pedestal temperature higher than 900eV, and electron pedestal pressure in the range 8–10kPa for the low-δ and 10–14kPa for the high delta-δ**.** The JET-ILW plasmas without N_2 seeding (red symbols) are characterized by a pedestal density in the range $6–8\ 10^{19} m^{-3}$, comparable to the JET-C data, but by $T_e^{ped} \approx 500–720$eV, which is approximately 20% lower than the coldest JET-C plasma considered. However, when N_2 is seeded into high-δ JET-ILW plasmas (green triangles), higher n_e^{ped} and T_e^{ped} can be reached with an electron pedestal pressure up to 11kPa, which is comparable to the JET-C plasmas. As discussed in reference [13], the rate of confinement improvement is dependent on the level of N_2 gas injected. This behaviour is significantly different for the low-δ JET-ILW plasmas. In this case, the seeding produces a slight reduction of the pedestal density and a slight increase of the pedestal temperature, with the pedestal pressure that remains unaffected to approximately 6kPa.

Concerning the ion temperature T_i, it has been verified $T_e = T_i$ for the JET-C shots. The JET-ILW shots with available T_i measurement have $T_e = T_i$ as well. All the JET-ILW shots have high collisionality [6], so a difference between T_e and T_i is not expected.

3. ELM TIME SCALES

The time evolution of electron temperature and density near the top of the pedestal (at $\rho_\theta = 0.95$) for three high-δ shots (a JET-C plasma, a non-seeded JET-ILW plasma and a JET-ILW plasma with N_2 seeding) are shown in figure 2. The temperature data are measured by the electron cyclotron emission (ECE) radiometer and the density data by the reflectometer.

The ELM effect is evident both by the drop in the electron temperature and density and by the increase in D_α signal. The temperature and density drops are approximately $\Delta T_e \approx 350$eV and $\Delta n_e \approx 1 \cdot 10^{19} m^{-3}$ for the JET-C shot, $\Delta T_e \approx 150$eV and $\Delta n_e \approx 1.5 \cdot 10^{19} m^{-3}$ for the JET-ILW shot without

N_2 seeding. For the JET-ILW shot with N_2 seeding the drops are between the JET-C shot and the JET-ILW shot.

To quantify the ELM time scale, figure 3 shows the time evolution of the temperature and density at at $\rho_\theta = 0.95$ for all the ELMs within a steady phase of the shot. A steady phase has been defined as a time interval at least 1s long with constant H_{98}, β_N, line averaged density and regular ELM frequency. The signals have been synchronized in order to have each ELM collapse at t = 0 and have been normalized to the pre-ELM value. Temperature data are from the ECE radiometer and density data from the reflectometer.

The ELM time scale is quantified by calculating the time interval from the beginning of the ELM collapse to the minimum after the collapse. This is calculated for each ELM within the steady phase of the shot and then averaged.

The minimum T_e for the JET-C shot is reached after approximately $\tau_{ELM} = 0.6 \pm 0.1$ms, figure 3(a). The density signal is significantly noisier resulting in a large uncertainty, with $\tau_{ELM} = 0.4 \pm 0.3$ms, figure 3(b).

The non-seeded JET-ILW shot has a behaviour significantly different from the non-seeded JET-C shot, see figure 3(c) and 3(d). First of all, two time scales can be identified both in the temperature and in the density. The first phase of the temperature collapse is very similar for all the ELMs, till $t\text{-}t_{ELM} \approx 1.8$ms. Then, the temperature starts to recover for approximately 40% of the ELMs, while a further collapse (even though with a slower decay rate) is present for the remaining ≈ 60% of the ELMs till $t\text{-}t_{ELM} \approx$ 10–15ms. The density signal is significantly noisier, but a similar behaviour is present. Note that these two time scales can be observed also in figure 2(d–f) whith the first ELM at t ≈ 16.38s significantly shorther than the second ELM at t ≈ 16.43s. Hereafter, to distinguish these two behaviours, the events corresponding to the short time scale are simply called ELMs, while the events corresponding to the longest time scale are called “slow transport events”. Sections 4 and 5 describe the behaviour of electron temperature and density during ELMs. Section 6 describes the behaviour of the slow transport events.

A second major difference between the JET-C shot and the JET-ILW shot is that the ELM time scale is significantly longer in the non-seeded JET-ILW shot ($\tau_{ELM} \approx 1.8$ms for the temperature and 2.5ms for the density) than in the JET-C shot ($\tau_{ELM} \approx 0.6$ms and 0.4ms).

The N_2 seeded JET-ILW shot shows a behaviour more similar to the JET-C than to the unseeded JET-ILW shot. As shown in figures 3(e) and 3(f), the slow transport events are not present and the ELM time scales are 0.9ms and 1.2ms, close to the JET-C shot.

The difference in the ELM time scale between the JET-C plasmas and the non-seeded JET-ILW plasmas is confirmed by quantifying τ_{ELM} for the shots described in Section 2. However, the reflectometer data were available only for a very limited number of JET-C shots.

The results are shown in figure 4 where the ELM time scale versus the pedestal stored energy is shown. τ_{ELM} is larger than 1.5ms for the non-seeded JET-ILW plasmas (red full symbols) and lower than 1ms for the JET-C plasmas (blue empty symbols). The seeded high-δ JET-ILW plasmas can

reach τ_{ELM} <1ms, a time scale that is comparable to the JET-C shots. It is important to highlight that for the low-δ plasma there is no clear correlation between τ_{ELM} and the pedestal energy. The τ_{ELM} range of variation is in fact very large, from 1ms to 2.5ms while the pedestal energy is approximately constant ($W_{ped} \approx 1MJ$). This suggests that the ELM time scale is not directly correlated to the pedestal energy. A further discussion is presented in Section 7.

4. PEDESTAL ELECTRON TEMPERATURE AND DENSITY COLLAPSE DURING ELMS

The electron temperature and density profiles are determined from the ECE radiometer and the reflectometer respectively. Pre-ELM profiles have been calculated by averaging all the profiles in a time window from –5ms to –1ms before the ELMs. Post-ELMs profiles have been calculated in an approximately 0.1ms long time window centered at the minimum of the signal after the ELM collapse (the time window is optimized from shot to shot). Figure 5(a) shows the average temperature profiles in the pre- and post-ELM intervals, red and blue lines respectively, for the non-seeded JET-ILW plasma 82540. Figure 5(b) shows the corresponding temperature profile collapse (thin black lines) during the ELM. The averaged density pre- and post-ELM profiles and the density collapse are shown in figures 5(c) and 5(d). ECE radiometer and/or reflectometer were not available for all the shots described in figure 1. In particular, the reflectometer data are available only for two JET-C shots. In these cases, the HRTS profiles have been used. Due to the low sampling frequency (20Hz), the HRTS cannot provide the profile evolution during a single ELM, so each measurement has been synchronized to its nearest ELM. The pre-ELM profiles have been obtained by considering the HRTS measurements in the time window from –10ms to –1ms before an ELM and the post-ELM profiles in a narrow time window after the ELM. This time window has been optimized from shot to shot and it is typically not longer than 0.5ms. When both ECE, reflectometer and HRTS are available, a good agreement is obtained within the uncertainty.

The maximum temperature collapse due to ELMs for the non-seeded JET-ILW plasma shown in figure 5 is $\Delta T_e \approx 150eV$ and the maximum density collapse $\Delta n_e \approx 2.0 \cdot 10^{19} m^{-3}$. The comparison of the electron temperature and density drops at the pedestal during ELMs for the JET-C and JET-ILW shots is shown in figure 6. The drops are calculated as difference between the pedestal height before the ELM and the pedestal height after the ELM. The temperature collapse is significantly lower in the non-seeded JET-ILW plasmas than in the JET-C plasmas, both for the high triangularity shots (figure 6a) and the low triangularity shots (figure 6b). When nitrogen is seeded into the high-δ JET-ILW plasmas, the temperature collapse can reach values comparable to the JET-C plasma, both in terms of absolute drops, with ΔT_e up to 350eV, and in terms of relative drops, with $\Delta T_e/T_e^{ped}$ up to 40–50%. When nitrogen is seeded into the low-δ JET-ILW plasma a marginal increase in the pedestal temperature is obtained, but the ELM temperature collapse remains significantly smaller than the JET-C shots.

The electron density drops are shown in figures 6(c) and 6(d). In the high-δ JET-C plasmas, note

the difference between the low Γ_{D2} shots (cyan triangles) and the shots with Γ_{D2} comparable to the JET-ILW plasmas (blue triangles). This is likely related to the difference in their pedestal height. The density pedestal drops in the non-seeded JET-ILW plasmas are significantly smaller than the JET-C plasmas with comparable Γ_{D2}. The seeded high-δ JET-ILW shots can reach density drops comparable to the JET-C, both in terms of absolute drops (Δn_e up to $2.5 \cdot 10^{19} m^{-3}$) and relative drops ($\Delta n_e/n_e^{ped}$ up to 20–25%). No major difference is observed in the low-δ JET-ILW plasmas with and without seeding, but the absolute drop is always larger than in JET-C low delta discharges.

5. ELM ENERGY LOSSES

The electron thermal energy is calculated by volume integrating the electron temperature and density profiles:

$$W_{th}^{e} = \frac{3}{2} k \int T_e n_e dV \tag{1}$$

The electron ELM energy losses are calculated as the W^{e}_{th} difference between the pre- and the post-ELM phase:

$$\begin{aligned} \Delta W_{ELM}^{e} &= \frac{3}{2} k \left[\int T_e n_e dV - \int \left(T_e - \Delta T_e \right) \left(n_e - \Delta n_e \right) dV \right] \approx \\ &\approx \frac{3}{2} k \left[\int \Delta T_e n_e dV + \int T_e \Delta n_e dV \right] = \Delta W_{cond}^{e} + \Delta W_{conv}^{e} \end{aligned} \tag{2}$$

where ΔT_e and Δn_e are the temperature and density collapses during the ELM, and ΔW^{e}_{cond}, ΔW^{e}_{conv} represent the conductive and convective losses respectively. The cross-term in equation 2 is negligible.

The total electron ELM energy losses versus the pedestal stored energy W_{ped} is shown in figure 7(a). The pedestal stored energy W_{ped} is calculated by considering both the electron pedestal pressure and the ion pedestal pressure using the HRTS for the electron and the charge exchange for the ions as described in [5]. For the JET-ILW plasmas $T_i = T_e$ is assumed.

ΔW^{e}_{ELM} is in the range 100–220kJ for the JET-C plasmas, significantly larger than the non-seeded ILW plasmas that are characterized by $\Delta W^{e}_{ELM} \approx$ 30–70kJ. The ELM energy losses for the JET-C plasmas are larger also in terms of the relative drop, with $\Delta W^{e}_{ELM}/W_{ped} \approx 6\%–10\%$, for the JET-C and $\Delta W^{e}_{ELM}/W_{ped} \approx 4\%–6\%$ for the JET-ILW.

JET-ILW plasmas can reach energy losses comparable to the JET-C when nitrogen is seeded. In this case, the JET-ILW have losses in the range $\Delta W^{e}_{ELM} \approx$ 40–130kJ and $\Delta W^{e}_{ELM}/W_{ped}$ up to 8%. Note that the JET-ILW shots with losses comparable to the JET-C are the plasmas which reach a W_{ped} comparable to the JET-C plasmas.

The contributions of the convective and conductive terms to the total ELM energy losses are shown in figure 9(b) and 9(c) respectively. The difference in the convective losses between JET-C

and JET-ILW plasmas is evident mainly for the high-δ shots, with ΔW^{e}_{conv} often larger than 50kJ in the JET-C and $\Delta W^{e}_{conv} < 50$kJ in the non-seeded JET-ILW. The difference is even more evident in the conductive losses with ΔW^{e}_{cond} 70–150kJ for the JET-C and ΔW^{e}_{cond} 20–50kJ for the JET-ILW. The ratio between the conductive losses and the pedestal energy increases from 2%–4% for the non-seeded JET-ILW plasmas to 4%–8% for the JET-C plasmas. The seeded JET-ILW plasmas with W_{ped} comparable to the JET-C plasmas have also comparable conductive losses.

Note that the ELM energy losses depend not only on the drops at the pedestal but also on the width of the ELM affected area. The ELM affected volume for the temperature seems marginally larger in the JET-C plasmas, with a radial width from $\rho_\theta \approx 0.8$ to $\rho_\theta \approx 1.0$ than in the non-seeded ILW plasmas, which have a radial width $\rho_\theta \approx 0.85$–1.0. No significant difference is observed in the ELM affected volume for the electron density. However, due to the large uncertainty in determining the width, conclusive claims are not possible.

6. THE SLOW TRANSPORT EVENT IN JET-ILW PLASMAS

An ELM in the JET-ILW plasma is often followed by a further transport event that occurs on a longer time scale. These events have been called "slow transport events", as discussed in Section 3. Figure 3(c) shows that the temperature collapse starts in a similar way for all the ELMs. The temperature starts to recover after 1.8ms for ≈ 40% of the ELMs while it continues to decrease up to ≈ 10ms after the ELM for the remaining 60% of the ELMs. The rate of reduction of the temperature is clearly lower during the second phase. The electron density has a relatively similar behaviour, as shown in figure 3(d).

These slow transport events can be relatively frequent in a JET-ILW plasma. Figure 8 shows the frequency of the slow transport events for all the shots analysed versus the pedestal stored energy. The frequency has been calculated for each shot as the number of the slow transport events, N_{slow}, divided by the total number of ELM collapses, N_{tot} (including both the standard ELMs and the ELMs followed by the slow transport event). The slow transport events can be present in up to 70% of the ELMs. However, the seeded JET-ILW plasmas with $W_{ped} > 1.5$MJ have no slow transport events. No ELM in JET-C is followed by a slow transport event.

Note that the pedestal stored energy alone is likely not the driving factor for the presence of the slow transport events. In particular, seeded JET-ILW plasmas with similar W_{ped} can have either no slow transport events or a large fraction of slow transport events. Apart from this behaviour, so far no other significant difference in the major plasma parameters has been observed. At the moment, the origin of the slow transport event is unclear.

It is important to observe that the slow transport event is not a back transition from a H-mode plasma to a L-mode plasma. First of all, net power across the separatrix, P_{sep} is above the L-H power threshold, $P_{L\text{-}H}$, as determined using the Martin scaling law [18]. In fact, $P_{L\text{-}H}$ is in the range 9–12MW and the $P_{sep}/P_{L\text{-}H} \approx 1.1$–$1.5$ for the present set of JET-ILW plasmas. Moreover, the pedestal structure is observed also at the maximum of the collapse both in the temperature and in

the density profiles. This is shown in figure 9, where the profiles before the ELM (red symbols) and at the maximum of the collapse during the slow transport events (blue symbols) are shown for the non-seeded JET-ILW shot 82540.

The slow transport event produces a further collapse of the pedestal density and temperature. For shot 82540, the temperature collapse is $\Delta T_e \approx 200$eV and the density collapse $\Delta n_e \approx 3 \cdot 10^{19} m^{-3}$ (see figures 9b and 9d), both larger than the collapses during the ELMs, which are $\Delta T_e \approx 150$eV and the density collapse $\Delta n_e \approx 2 \cdot 10^{19} m^{-3}$ (see figures 5b and 5d). These results are summarized in figure 10, where in frame (a) and (b) the temperature and density collapses at the pedestal are shown versus the pedestal temperature and density. For reference, the temperature and density collapses during ELMs are shown as well. On average, the temperature collapses due to the slow transport event are larger than the ELM collapse. The density drops due to the slow transport event are significantly larger than those due to ELMs, with relative drops ≈ 30%–50% while the ELM density drops are lower than 25%. The total electron energy losses are shown in figure 10(c). The losses due to the slow transport event can reach up to 10% of the pedestal stored energy and are significantly larger than the ELM energy losses in the JET-ILW plasmas.

7. DISCUSSION

The nitrogen seeded JET-ILW plasmas can have an ELM behaviour similar to the JET-C plasmas both in terms of energy losses and ELM time scales. While the ELM energy losses seem well correlated with the pedestal stored energy, the ELM time scale does not seem to be strongly correlated with W_{ped}. In particular, as shown in figure 4(a), the low-δ JET-ILW plasmas have a large range of variation in the ELM time scale, while W_{ped} is constant. This section investigates possible parameters that might regulate the behaviour of the ELM energy losses and the ELM time scale.

Earlier works [16, 17, 2, 3] have shown that the relative ELM energy losses scale with the pedestal collisionality ν_e^*(neo). The collisionality is defined as $\nu_e^*(\text{neo}) = qR^{5/2}a^{-3/2}(\lambda_{ee})^{-1}$ where $\lambda_{ee} = 1.7 \times 10^{17} T_e^2(\text{eV})/[n_e(m^{-3}) \ln\Lambda]$ is the electron-electron Coulomb collision mean free path, with the temperature and density calculated at the pedestal [17].

The present results are compared with those described in [17] in figure 11 which shows the total ELM energy losses ΔW_{ELM} relative to the total pedestal stored energy W_{ped} versus the pedestal collisionality. For the present data set, the total ELM energy losses ΔW_{ELM} have been calculated using the electron ELM energy losses ΔW^e_{ELM}, assuming $T_e = T_i$ and calculating the ion density from the line integrated effective charge using as main impurity carbon for the JET-C plasmas ($n_i = n_e(7–Z_{eff})/6$), beryllium for the non-seeded JET-ILW plasmas ($n_i = n_e(5–Z_{eff})/4$) and nitrogen the seeded JET-ILW plasmas ($n_i = n_e(8–Z_{eff})/7$). The present data set follows reasonably well the earlier trend of the relative ELM energy losses versus the pedestal collisionality. In particular, the JET-ILW plasmas have energy losses comparable with the JET-C when their pedestal collisionality is reduced to the JET-C values.

For comparison, the energy losses due to the slow transport events are shown in figure 11 as

black squares. The slow transport events do not fit into the trend of $\Delta W_{ELM}/W_{ped}$ versus ν_e^*(neo) and are significantly larger than the JET-ILW ELM energy losses.

The pedestal collisionality seems to be a good ordering parameters also for the ELM time scale. Figure 12 shows the correlation between τ_{ELM} and the pedestal collisionality. A positive trend is present for both the high-δ and low-δ plasmas. In particular, the time scale of the low-δ JET-ILW plasmas is better correlated to the pedestal collisionality than to the pedestal stored energy (figure 4a). Note that all the JET-C plasmas analysed have the same collisionality and the same ELM time scale.

The confinement improvement with nitrogen seeding has been observed also in ASDEX Upgrade where it is associated with the correlation between H_{98} and the effective charge Z_{eff} [26]. So far, in JET-ILW, a strong correlation between confinement and Z_{eff} has not been observed yet [13]. Nonetheless, the increase of the N_2 seeding rate produces an increase in Z_{eff} [13]. The N_2 seeded JET-ILW plasmas analysed in this work have a seeding rate in the range $\Gamma_{N2} = 0.5–3\cdot10^{22}$ (e/s). The seeded shots with low Γ_{N2} have Z_{eff} comparable to the non-seeded JET-ILW plasmas ($Z_{eff} \approx$ 1.3–1.4), while with high Γ_{N2} $Z_{eff} \approx 1.6$ which is comparable to the JET-C plasmas [13].

To investigate if the ELM properties are related to the change in Zeff, figure 13 shows the ELM time scale, the ELM energy losses and the fraction of slow transport events versus Z_{eff}. The ELM time scale for the JET-ILW plasmas seems indeed well correlated with the effective charge. The seeded JET-ILW shots with $Z_{eff} > 1.5$ have a time scale comparable to the JET-C shots. On the other hand, there is no correlation for the JET-C plasmas, for which the ELM time scale is relatively constant but Z_{eff} varies from 1.6 to 2.2. In this sense, the ELM time scale is better correlated with the pedestal collisionality since the JET-C plasmas which have similar ν_e^*(neo) have a similar τ_{ELM}. However, we cannot exclude that the effective charge is related to the ELM time scale via other plasma parameters, such as the resistivity. Figure 13(b) shows the time scale versus the resistivity, calculated as $\eta = 1.6\cdot10^{-9}\ \ln\Lambda\ Z_{eff}/(T^e_{ped})^{3/2}$. While the JET-ILW plasmas show a positive correlation with η, the JET-C shows no clear correlation between ELM time scale and resistivity.

Concerning the ELM energy losses, a weak positive trend with Z_{eff} is present, figure 13(c). In particular, JET-C plasmas have large Z_{eff} and large energy losses while non-seeded JET-ILW shots have smaller Z_{eff} and smaller energy losses. However, the seeded JET-ILW plasmas show no clear correlation between energy losses and Z_{eff}. The correlation between the energy losses and the plasma resistivity is not strong either, see figure 13(d).

As a final comment, even if the the slow transport events are present only in the JET-ILW plasmas, no clear correlation is found with Z_{eff} or with the resisitivity. This is shown in figures 13(e) and 13(f). In fact, JET-ILW plasmas with $Z_{eff} \approx 1.4$ can be characterized by a large fraction of slow transport events or by no slow transport.

CONCLUSION

This work describes the N_2 seeding effect on the ELM time scale and on the ELM energy losses in JET-ILW and compares the results with similar non-seeded JET-C plasmas.

The ELM energy losses in the non-seeded JET-ILW plasmas are clearly smaller than in the JET-C plasmas, both concerning the absolute losses and the relative losses ($\Delta W^{e}_{ELM}/W_{ped} \approx 4\%–6\%$ for the non-seeded JET-ILW and $\approx 6\%–10\%$ for the JET-C). So far, JET-ILW plasmas with pedestal heights comparable to the JET-C have been obtained only by seeding nitrogen. In these cases, JET-ILW shots show energy losses similar to the JET-C shots.

The ELM time scale shows a major difference between non-seeded JET-ILW and JET-C as well. First of all, the JET-ILW ELM collapse is often followed by a further collapse, even though with a longer time scale. These slow transport events are not present in the JET-C and disappear in the N_2 seeded JET-ILW shots that have pedestal heights comparable to the JET-C. However, no clear trend between the frequency of these events and the pedestal parameters has been observed. The origin of the slow transport events is still unclear. Second, while the ELM time scale is larger in the non-seeded JET-ILW plasmas ($\tau_{ELM} > 1.5$ms) than in the JET-C ($\tau_{ELM} \approx 0.6$ms), the seeded JET-ILW plasmas can reach times time scales lower than 1ms and comparable to the JET-C ones.

The difference in ELM energy losses between the non-seeded JET-ILW plasmas and the JET-C plasmas is probably not a direct effect of the difference in the pedestal height. Instead, the low pedestal temperature of the JET-ILW shots is reflected into a pedestal collisionality higher than the in JET-C. Due to the high pedestal collisionality, the non-seeded JET-ILW plasmas have energy losses lower than the corresponding JET-C shots. When N_2 seeding increases the JET-ILW pedestal temperature to values comparable to the JET-C, a comparable collisionality is achieved as well. As a consequence, the JET-ILW ELM energy losses are also comparable to the those in the JET-C. The pedestal collisionality seems to be a reasonable ordering parameters also for the ELM time scale. However, the physics reason behind the lower pedestal temperature in the non-seeded JET-ILW and the role of nitrogen in the confinement improvement is still under investigation and it has not been identified yet.

Finally, the presence of the slow transport events could have in principle modified the predictions of the ELM energy losses in ITER. The slow transport events have in fact energy losses twice as large as those obtained in the earlier ELM studies (figure 11). However, the slow transport events disappear in the N_2 seeded shots once the JET-ILW recovers a pedestal comparable to the JET-C. This suggest that the slow transport events might be not a major problem for ITER. Excluding the slow transport events, the JET-ILW data fits well within the earlier scaling of the ELM energy losses with the pedestal collisionality.

ACKNOWLEDGEMENT

This work was supported by EURATOM and carried out within the framework of the European Fusion Development Agreement. The views and opinions expressed herein do not necessarily reflect those of the European Commission.

REFERENCES

[1]. L. Barrera, E. de la Luna, L. Figini et al., Plasma Physics and Controlled Fusion **52**, 085010 (2010)

[2]. M.N.A. Beurskens, T.H. Osborne, L.D. Horton et al., Plasma Physics and Controlled Fusion **51** 124051 (2009)

[3]. M.N.A. Beurskens, A. Alfier, B. Alper et al., Nuclear Fusion **49** 125006 (2009)

[4]. M.N.A. Beurskens, L. Frassinetti, C. Challis et al., "24th IAEA Fusion Energy Conference", San Diego, USA, 2012, pp EX/P7-20.

[5]. M.N.A. Beurskens, L. Frassinetti, C. Challis et al., Nuclear Fusion **53** 013001 (2013)

[6]. M.N.A. Beurskens, L. Frassinetti, C. Challis et al., Nuclear Fusion **54** 043001 (2014).

[7]. M.N.A. Beurskens, J. Schweinzer, C. Angioni et al., Plasma Physics and Controlled Fusion **55**, 124043 (2013)

[8]. S. Brezinszek et al., "24th IAEA Fusion Energy Conference", San Diego, USA, 2012, pp EX/4-1.

[9]. E. de la Luna et al., Review of Scientific Instruments **74**, 1414 (2003)

[10]. L. Frassinetti, M.N.A. Beurskens, R. Scannell et al., Review of Scientific Instruments **83**, 013506 (2012)

[11]. C. Giroud, M. Oberkofler, D. Douai et al., "24th IAEA Fusion Energy Conference", San Diego, USA, 2012, pp EX/P5–30.

[12]. C. Giroud, G. Maddison, K. McCormick et al., Nuclear Fusion **52** 063022 (2012)

[13]. C. Giroud, G.P. Maddison, S. Jachmich et al., Nuclear Fusion **53** 113025 (2013)

[14]. ITER Physics Basis, Nuclear Fusion **39**, 2175 (1999)

[15]. M.J. Leyland, M.N.A. Beurskens, L. Frassinetti et al., Nuclear Fusion **53** 083028 (2013).

[16]. A. Loarte, M. Becoulet, G. Saibene, et al., Plasma Physics and Controlled Fusion **44** 1815 (2002)

[17]. A. Loarte, G. Saibene, R. Sartori et al., Plasma Physics and Controlled Fusion **45** 1549 (2003)

[18]. Y. Martin et al., Journal of Physics: Conference Series **123** 012033 (2008)

[19]. G. Matthews et al., Journal of Nuclear Materials **438**, S2 (2013)

[20]. R. Neu et al., Physica Scripta 014038 (2009)

[21]. I. Nunes, P.J. Lomas, D.C. McDonald et al., 23th IAEA Fusion Energy Conference, Daejong, Republic of Korea, 2010, EXC/P8-03.

[22]. R. Pasqualotto, P. Nielsen, C. Gowers et al., Review of Scientific Instruments **75**, 3891 (2004).

[23]. G. Saibene, R. Sartori, A. Loarte, et al., Plasma Physics and Controlled Fusion **44** 1769 (2002)

[24]. R. Sartori, G. Saibene, L.D. Horton et al., Plasma Physics and Controlled Fusion **46**, 723 (2004)

[25]. P.A. Schneider, E. Wolfrum, M.G. Dunne et al., Plasma Physics and Controlled Fusion **56**, 025011 (2014)

[26]. J. Schweinzer, A.C.C. Sips, G. Tardini et al., Nuclear Fusion **51** 113003 (2011)

[27]. A. Sirinelli, B. Alper, C. Bottereau, et al., Review of Scientific Instruments **81**, 10D939 (2010)
[28]. E. Wolfrum et al., Plasma Physics and Controlled Fusion **53** 085026 (2011)
[29]. Zhitlukin et al., Journal of Nuclear Materials **363**, 301 (2007)

	δ	**Ip(kA)**	**B(T)**	**P_{NBI}(MW)**	**$\Gamma_{D2}10^{22}$(e/s)**	**f_{ELM}(Hz)**	**n_e/n_{GW}**	**ELM**
ILW	0.4	2.5	2.7	15–17	2.5±0.8	28±14	0.78±0.04	type I
ILW+N2	0.4	2.5	2.7	15–17	2.1±0.9	40±15	0.92±0.06	type I
CFC	0.4	2.5	2.7	15–17	2.3±0.5	10±3	0.92±0.06	type I/II
CFC (low gas)	0.4	2.5	2.7	15–17	0.3±0.1	22±3	0.71±0.04	type I
ILW	0.2	2.5	2.7	15–17	1.6±0.7	33±15	0.73±0.03	type I
ILW+N2	0.2	2.5	2.7	15–17	1.1±0.3	35±6	0.56±0.03	type I
CFC	0.2	2.5	2.7	15–17	0.8±0.5	33±11	0.67±0.03	type I

Table 1: Triangularity, current, magnetic field, input power, D_2 gas rate, ELM frequency, pedestal density relative to the Greenwald desnity and ELM type of the shots analysed.

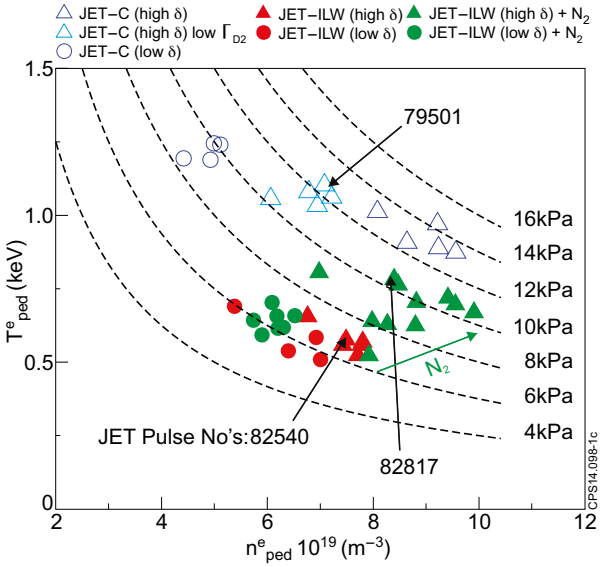

Figure 1: Electron pedestal temperature and density for JET-C (empty symbols) and JET-ILW (full symbols) plasmas in the pre-ELM phase. JET-ILW plasmas with N_2 seeding are in green. High-δ shots are represented with triangles and low-δ with circles. The dashed lines highlight the corresponding electron pedestal pressure. The green arrow highlights the increase of N_2 flow.

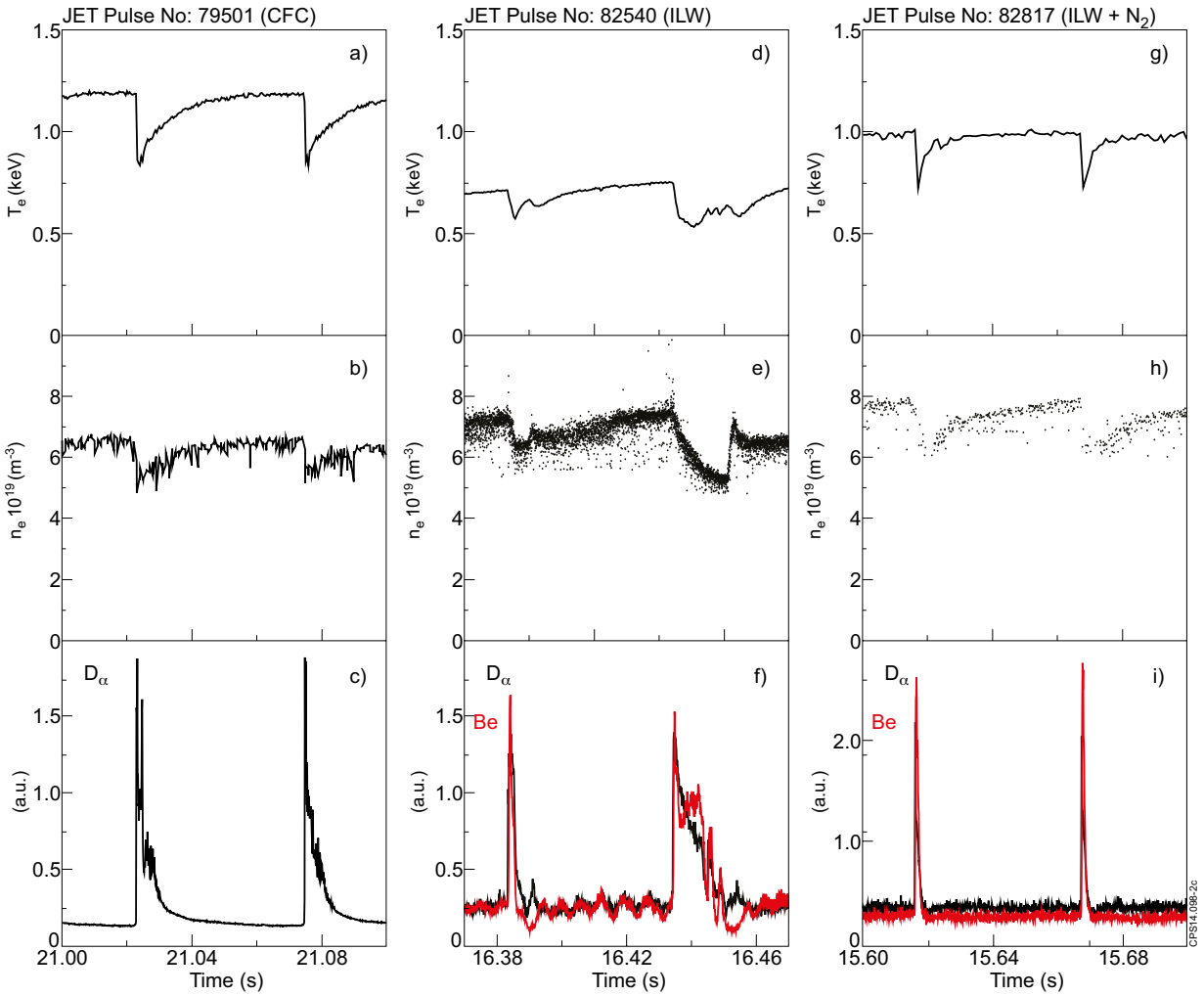

Figure 2: Time evolution at ρ_θ =0.95 in a 0.1s time window of electron temperature (first row), electron density (second row) and D_α signal (third row) for a high-δ JET-C shot (first column), a high-δ JET-ILW without N_2 seeding (second column) and a high-δ JET-ILW with N_2 seeding (third column).

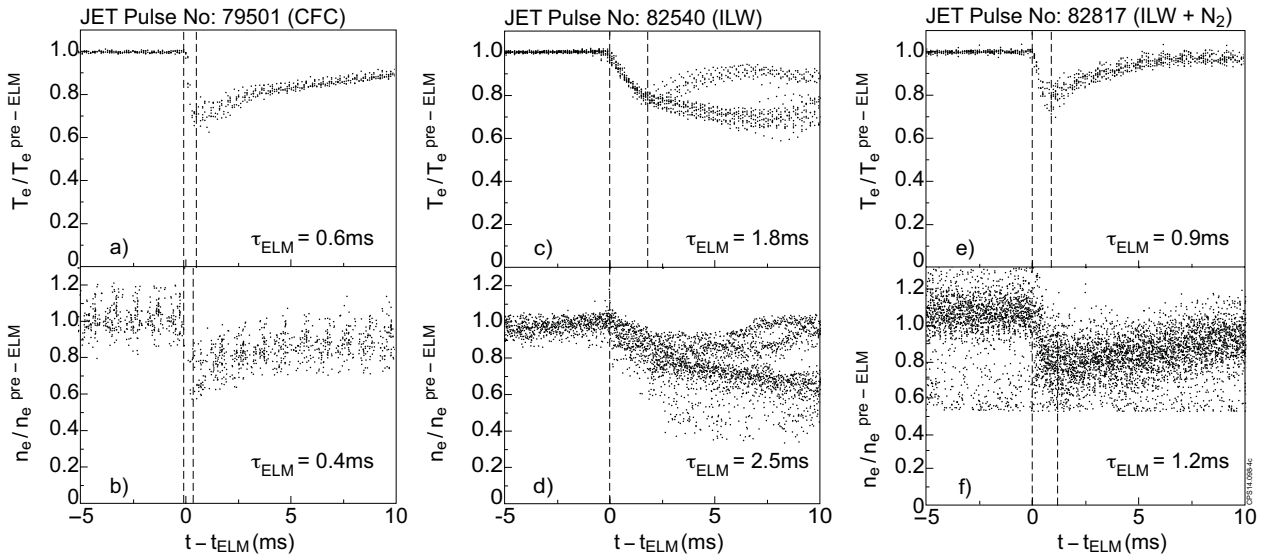

Figure 3: Time evolution ELM synchronized of electron temperature (first row) and electron density (second row) at r_θ =0.95 for a high-δ JET-C shot (first column), high-δ JET-ILW with no N_2 seeding (second column) and high-δ JET-ILW with N_2 seeding (third column).

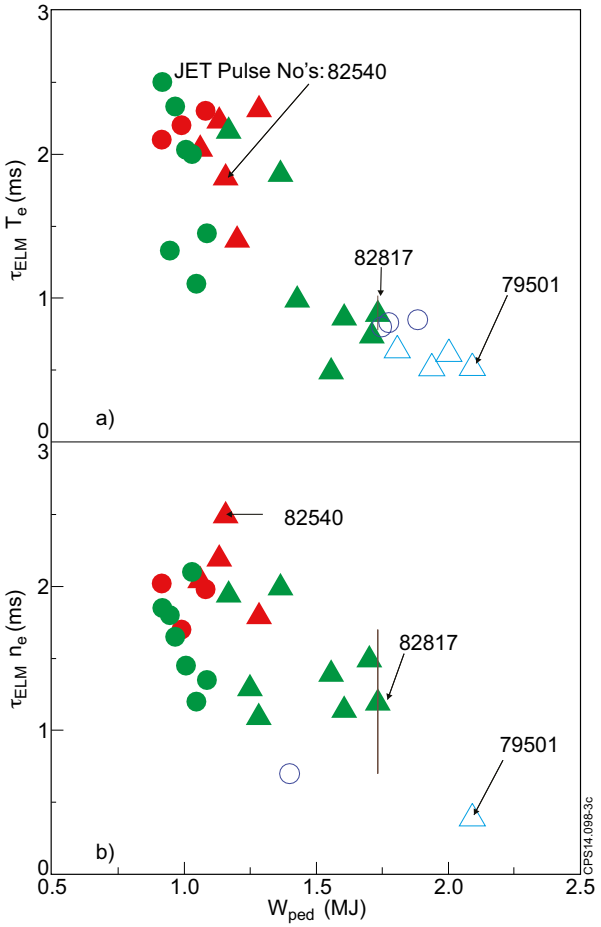

Figure 4: ELM time scale τ_{ELM} versus the pedestal energy W_{ped} for the temperature collapse (a) and for the density collapse (b). The time scales are calculated with the ECE radiometer and the reflectometer respectively. The pedestal energy is calculated using the HRTS as described in section 5. The typical error bars are in the range 0.1–0.4ms for the electron temperature and 0.4–0.8ms for the electron density (error bars are shown for the 82817 shot only). Symbols and colour code as in figure 1.

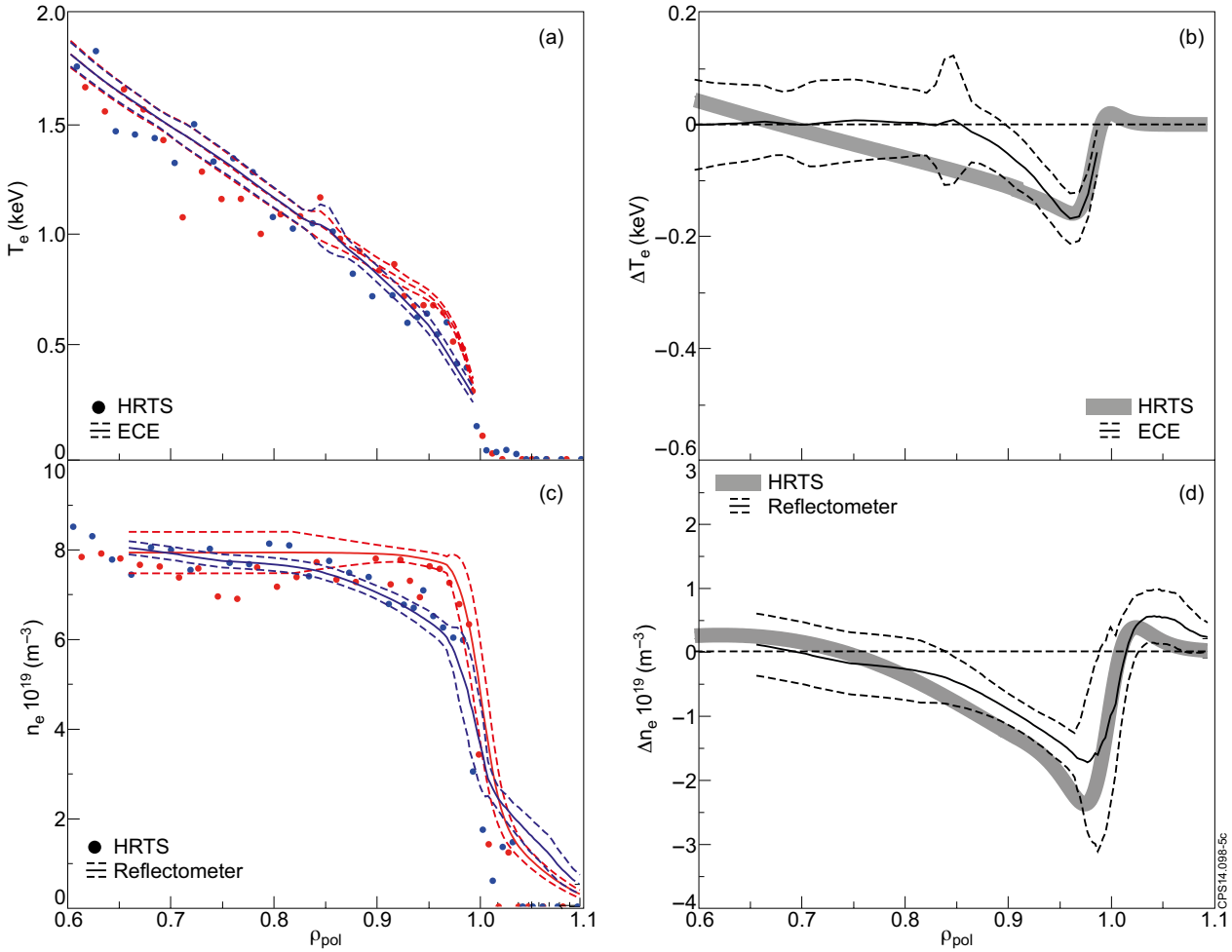

Figure 5: Profiles for the non-seeded JET-ILW plasma 82540. (a) Electron temperature profiles before (red) and after (blue) the ELM as measured by the HRTS (dots) and by the ECE radiometer. The continuous lines represent the average of the ECE profiles and the dashed lines represent the spread of the profiles. (b) Profile of the temperature collapse during the ELM as measured by the ECE (thin black lines) and by the HRTS (thick grey line). The HRTS temperature collapse is calculated from the pre- and post-ELM fits obtained with a modified hyperbolic tangent function. Frame (c) and (d) show the density profiles and the density collapse as measured by the reflectometer (lines) and the HRTS (dots).

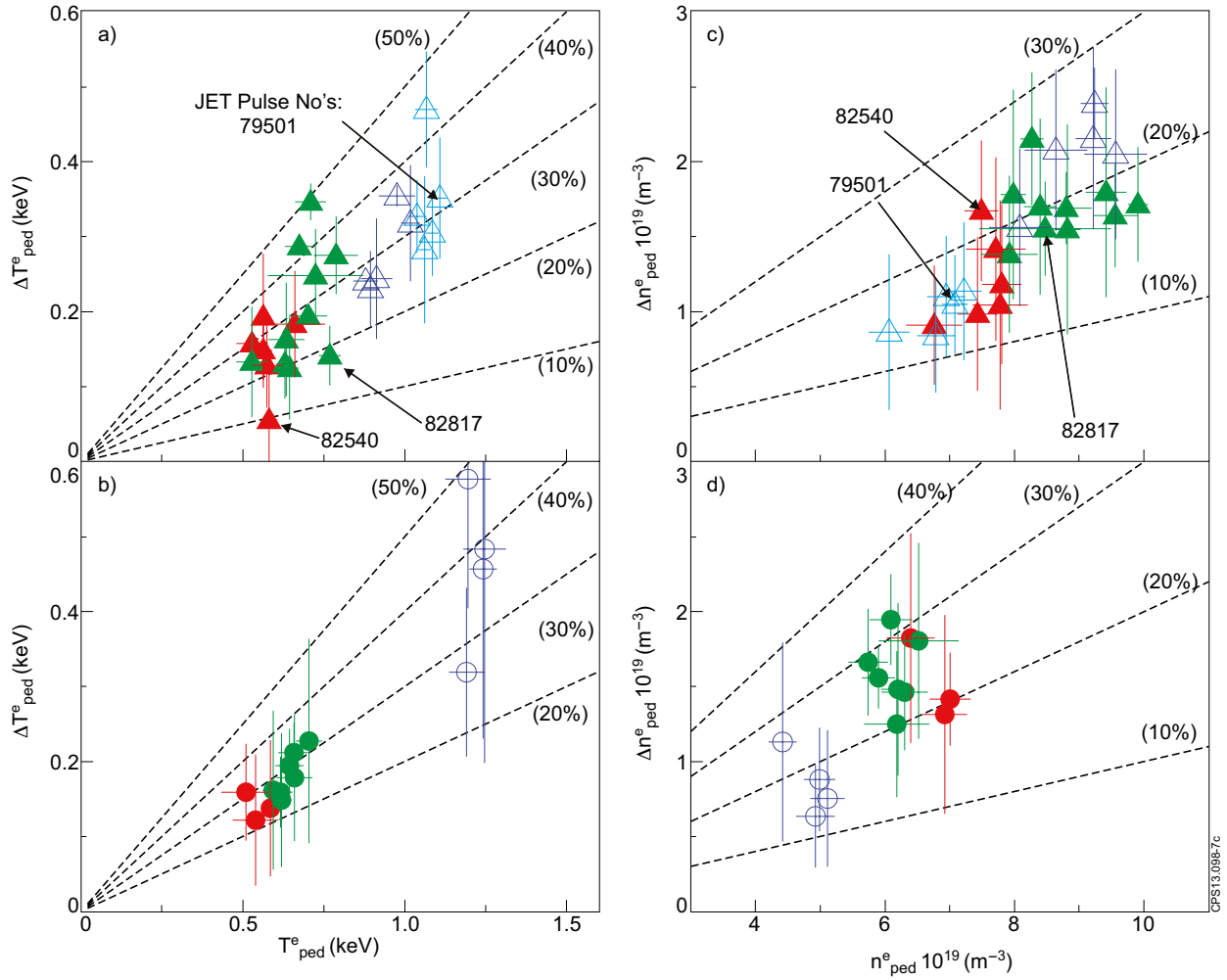

Figure 6: Electron temperature drop at the pedestal during ELMs versus the pedestal temperature for high and low triangularity plasmas, frames (a) and (b) respectively. Electron density drop at the pedestal versus the pedestal density for high and low triangularity plasmas, frames (c) and (d) respectively. The dashed lines show constant ratios between the pedestal drop and the pedestal value.

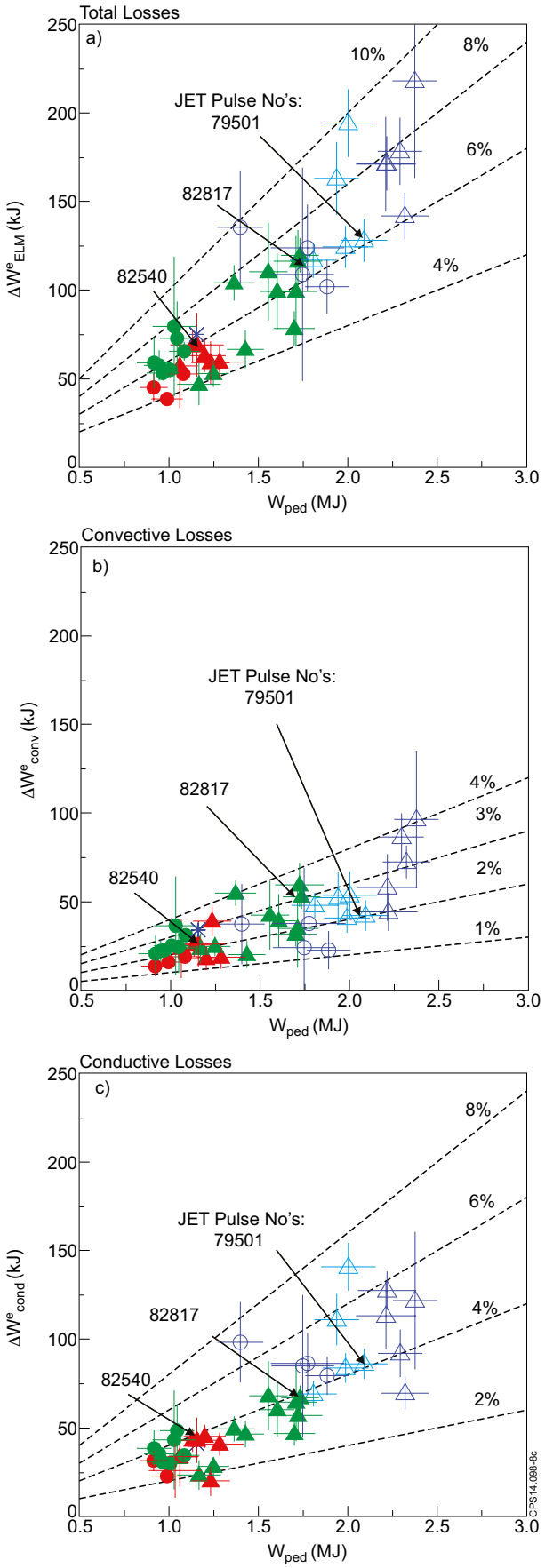

Figure 7: Electron ELM energy losses versus pedestal stored energy for the total losses (a), the convective losses (b) and the conductive losses (c). The dashed lines highlight constant ratios of the ELM losses versus the pedestal stored energy.

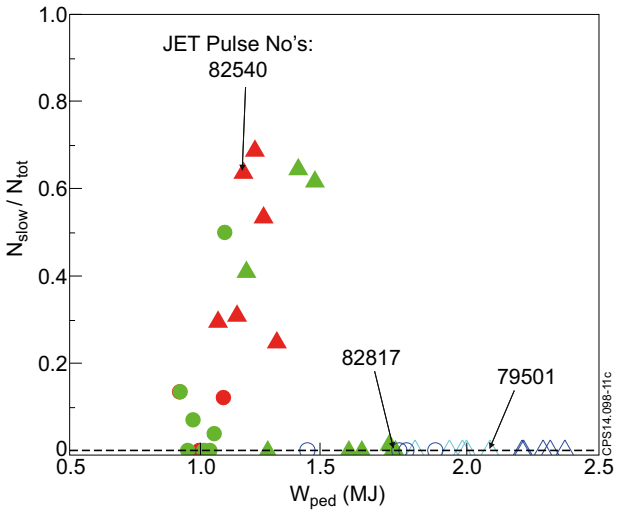

Figure 8: Ratio between the number of slow transport events and the total number of ELMs (including both standard ELMs and those followed by the slow transport event) versus the pedestal energy.

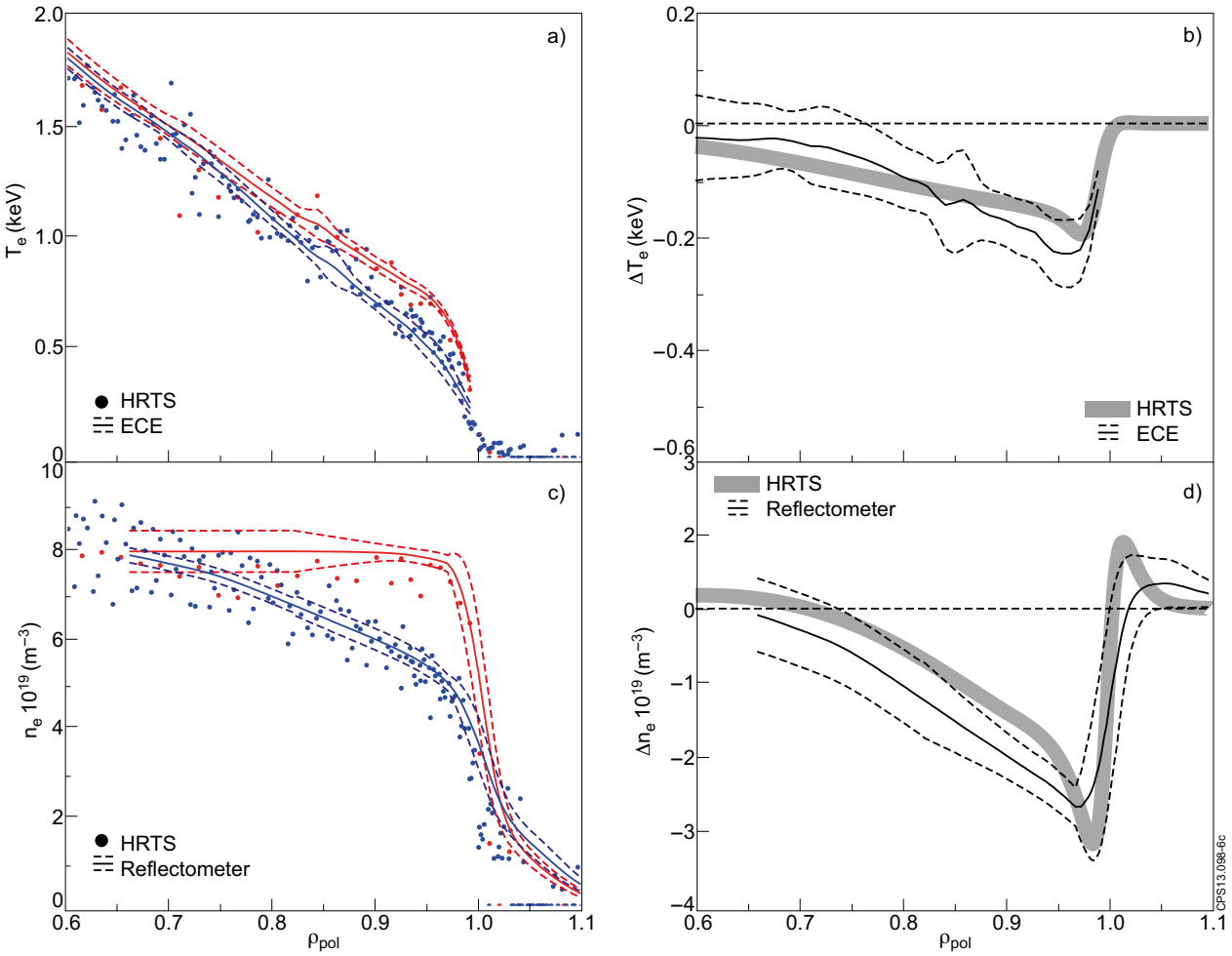

Figure 9: Profiles in the pre-ELM phase and after the slow transport event for the non-seeded JET-ILW plasma 82540. Pre-ELMs profiles, red data in frames (a) and (c), are calculated in time window from –5ms to –1ms before the ELMs. Post-ELMs profiles, blue data in frames (b) and (d), have been calculated in an approximately 0.5ms long time window centered at the minimum of the signal after the beginning of the slow transport event. The profiles of the temperature and density collapses are shown in frame (b) and (d) respectively.

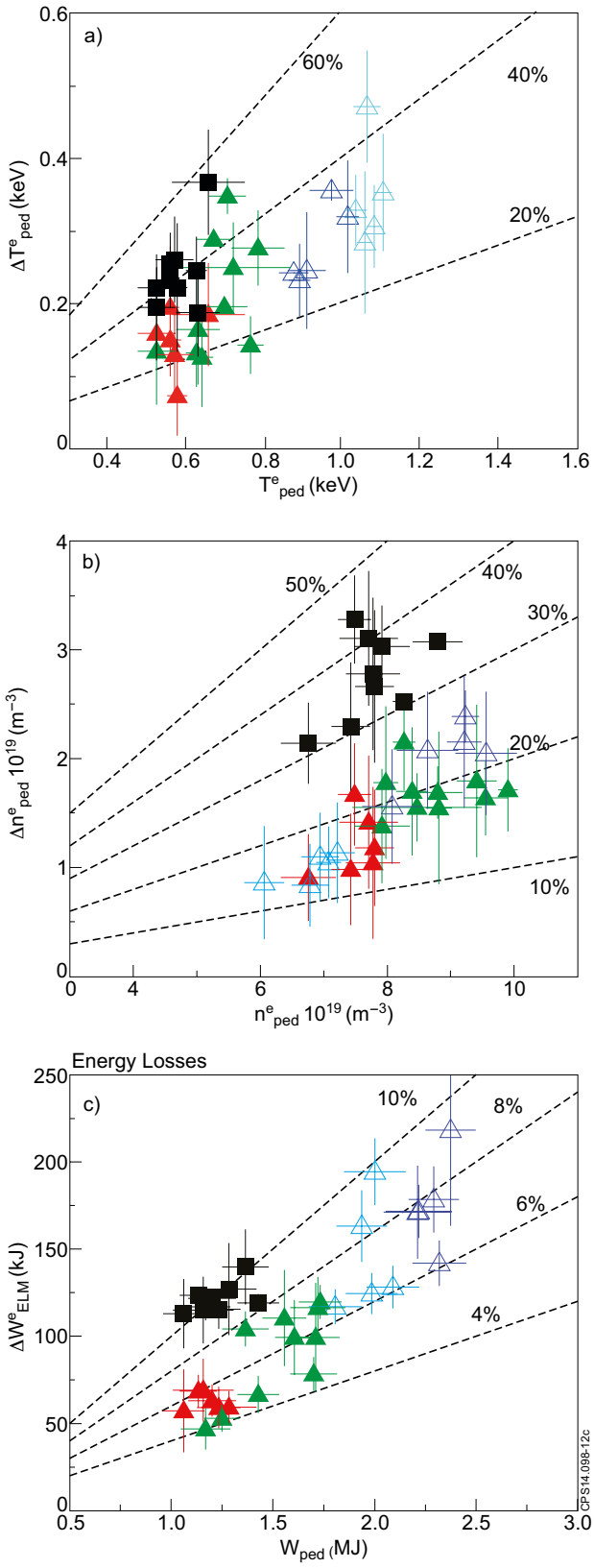

Figure 10: Pedestal drops for electron temperature (a) and density (b) versus the pre-ELM pedestal value. Electron energy losses versus the pedestal energy (c). Black squares highlight the drops due to the slow transport events. Coloured symbols highlight the drops due to the ELMs.

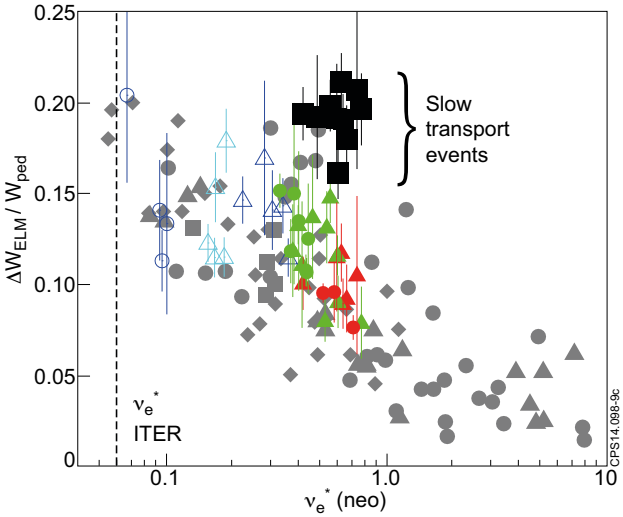

Figure 11: Relative ELM energy losses versus the pedestal collisionality for the present sets of JET-C data (blue and cyan symbols), non-seeded JET-ILW data (red) and seeded JET-ILW data (green). The black squares highlight the energy losses during the slow transport events in the JET-ILW plasma. The grey data show the multi-machine results described in [Loarte PPCF 2003].

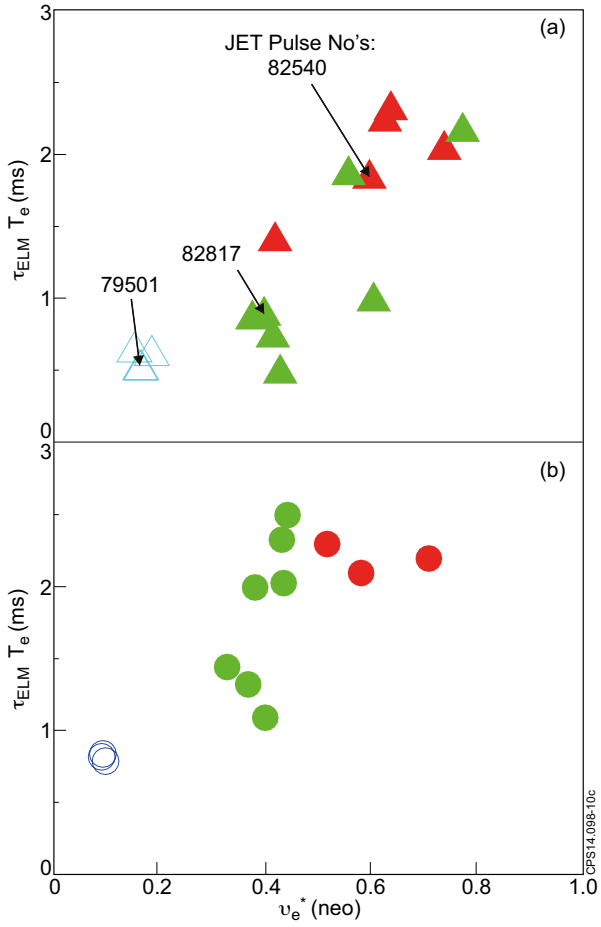

Figure 12: Temperature *ELM time scale versus pedestal collisionality for the high-δ plasma (a) and the low-δ plasmas (b).*

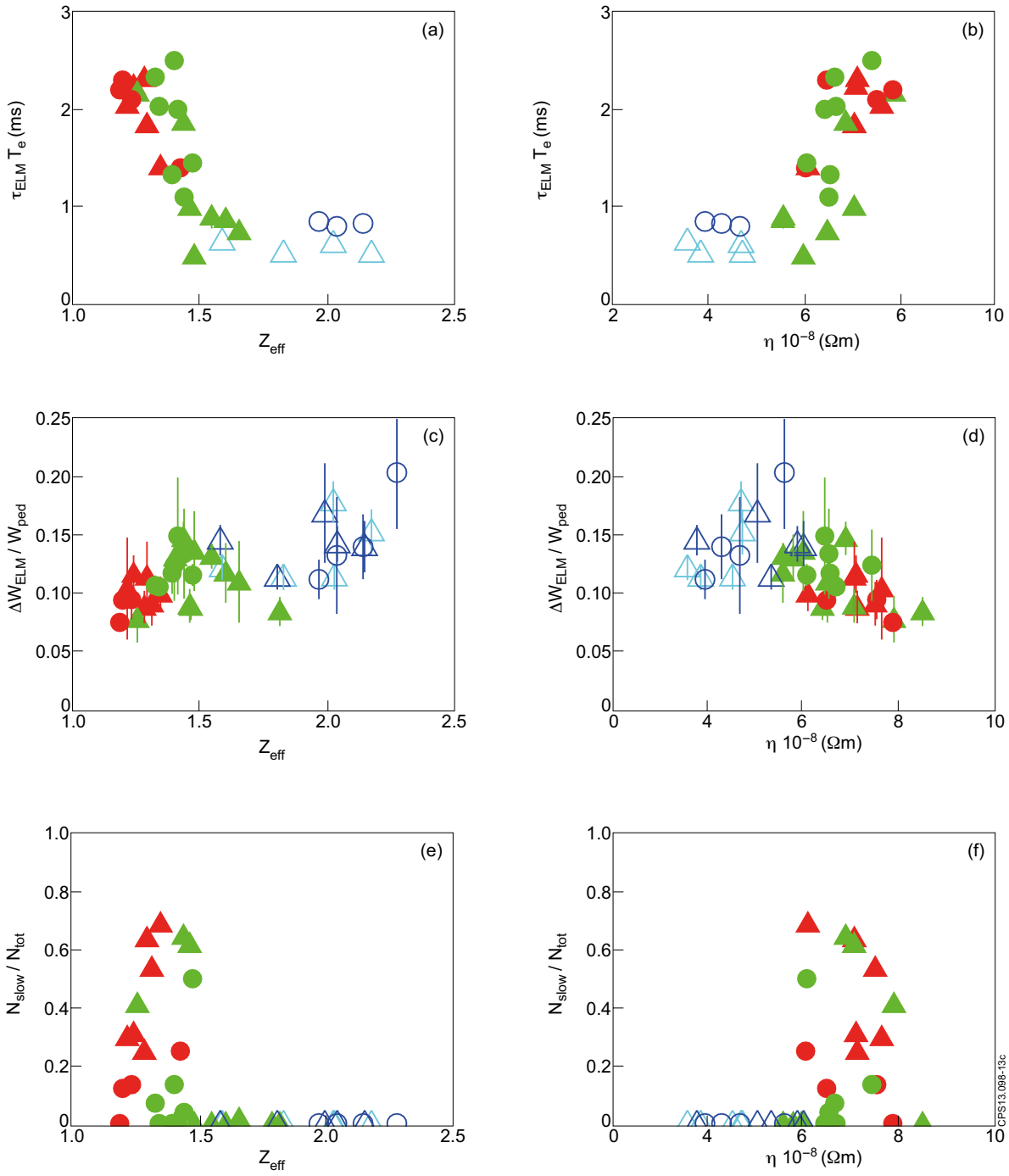

Figure 13: ELM time scale (a) and (b), ELM energy losses (c) and (d), fraction of slow transport events (e) and (f) versus the effective charge (left columns) and the plasma resistivity (right column).